Seismic reservoir characterization and pressure depletion of the Abu Madi Formation in the NW Khilala field, onshore Nile Delta, Egypt

Nadia Abdel FATTAH[1] (iD), Ibrahim Mohamed IBRAHIM[2] (iD), Manal ELKAMMAR[1,*] (iD)

[1] Geophysics Department, Faculty of Science, Cairo University, Egypt

[2] Geophysics consultant

Abstract: The Late Messinian Abu Madi Formation represents the most prospective deep reservoir target in the Nile Delta. Hydrocarbon exploration in the Nile Delta over the last few decades has been targeted to understand the Abu Madi reservoir quality and distribution. The integration of rock physics, amplitude versus angle (AVA), seismic interpretation, seismic attributes, and seismic inversion could successfully determine the characteristics of the late Messinian Abu Madi Formation in the North West Khilala (NWKh) field, which is located in the central onshore part of the Nile Delta, Egypt. The NWKh field is located on the eastern margin of the Disouq concession close to producing the West Khilala (WKh) field, with highly heterogeneous reservoir parameters. The reservoir is classified as lacustrine turbidites deposited in semi-isolated Late Messinian Basins. The Abu Madi Formation can be subdivided into upper and lower sand members. It is very common that they are separated by an intraformational shale layer. AVA analysis performed on the top of the Abu Madi reservoir suggested a class 2p. Seismic data were inverted to delineate the overall lateral extent of the reservoir. The prestack inversion process was integrated with rock physics modelling of the wells to generate high-resolution multiple rock property models to characterize the reservoir and observe or investigate different pressure depletion trends. The pressure depletion of the lower Abu Madi in the North West Khilala field was investigated laterally and vertically by the relative/full spectrum inversion and formation modular dynamic tester (MDT) pressure data, respectively. This depletion is due to communication with the West Khilala field, which was produced from the Lower Abu Madi (LAM) sand interval in 2007.

Key words: rock physics, reservoir chracterization, AVA and pre-stack inversion, seismic attributes, Abu Madi Formation

1. Introduction

The Nile Delta with its recent great onshore and offshore gas discoveries

---

*corresponding author, e-mail: manal@sci.cu.edu.eg

(e.g., Zohr, Noras) is currently known as the most prolific gas province in North Africa and is considered one of the most significant deltas for deep petroleum exploration (*EGPC, 1994; Abdel Aal et al., 1994; Dolson et al., 2005*). The quality of the Abu Madi reservoir facies is largely controlled by their initial depositional conditions, whereas the post depositional attributes play a relatively minor role (*Salem et al., 2005; Leila et al., 2019*).

The first discoveries were made in the late 1960s and were concentrated along the Abu Madi Valley trend (*Rizk et al., 2002*). A number of fields were subsequently discovered with the north–south trending incised valley trend. However, following a phase of extensive 3D seismic acquisition and interpretation several fields have been discovered since 2007. Most discoveries have been made on structurally controlled traps, which usually include some stratigraphic trapping elements (facies changes and sand pinch-out). All discoveries were associated with positive AVO responses, which generally followed the mapped structural traps (*Vaughan et al., 2014*).

The main objective of this paper is to study the reservoir characteristics to develop the Late Messinian Abu Madi Formation (LMAMF), which is a prolific producing gas reservoir in the North West Khilala concession located in the onshore part of the central Nile Delta, Egypt (Fig. 1), and to
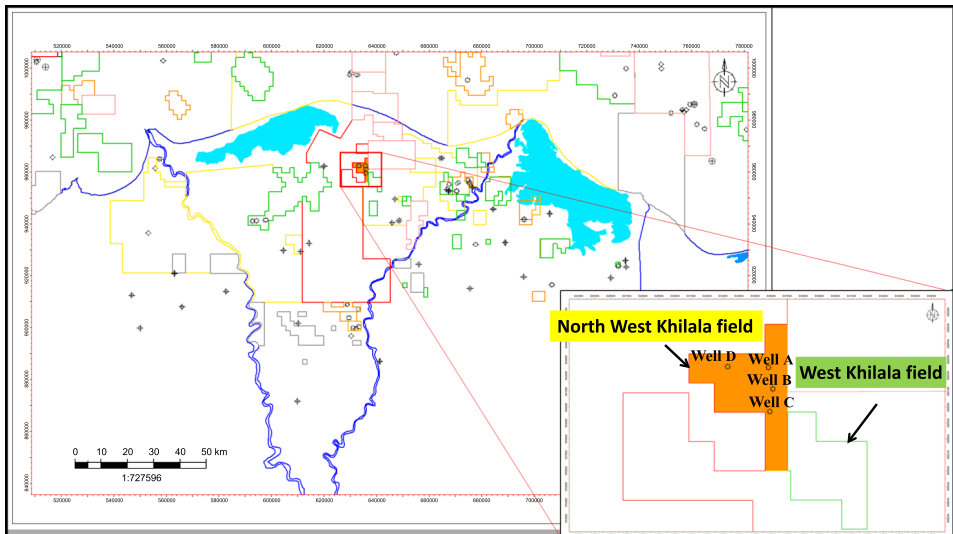

Fig. 1. Location map of North West Khilala field in onshore Nile Delta, Egypt.

study the depletion of the lower Abu Madi sand interval.

The Abu Madi Reservoir in the West Khilala field started production in 2007 and was subsequently appraised during 2010 and 2011 in the northwest Khilala Field. The drilling history of Well A and Well B is that they were drilled before production from a nearby field (West Khilala (WKh) field) in 2007. Well A was reappraised again during production from the North West Khilala field, and then Well C and Well D were drilled (Fig. 2).
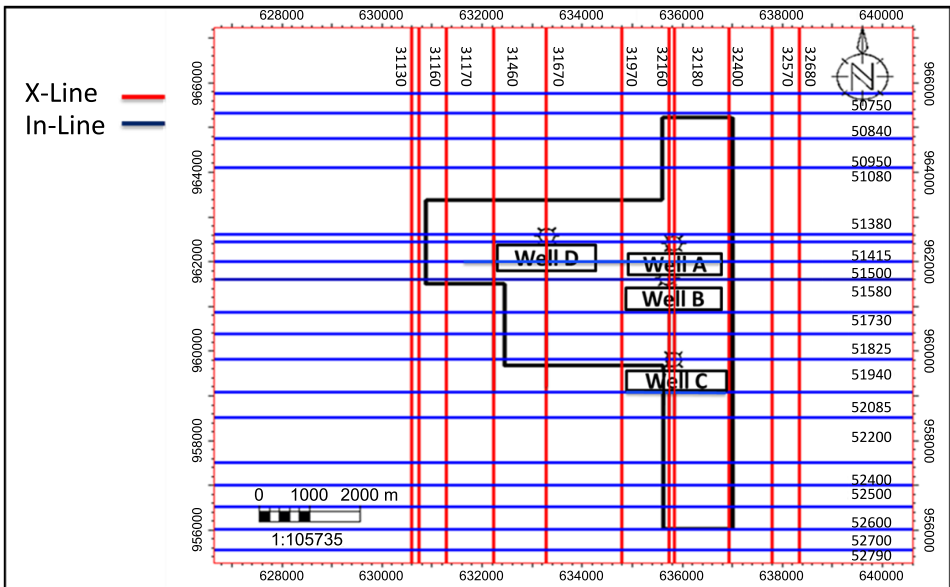

Fig. 2. The available data in the study area.

The North West Khilala closure comprises a 3-way dip structure against a N–S to NNW–SSE trending an echelon normal fault that is downthrown to the east and northeast (internal reports). In the present study, the sub-surface dataset (Fig. 2) consists of four wells that encounter the target and 30 2D seismic lines (including full stacks and near- and far-angle stacks), which help provide reservoir models in the North Western Khilala field. The dataset was analysed and interpreted to achieve the study objectives. Seismic inversion and AVA have been successfully applied during the exploration phase of LMAMF in the onshore Nile Delta. The integration of relative and full-spectrum prestack Inversion, AVA, seismic attributes, and rock physics

modelling was successfully applied to characterize the Abu Madi reservoir and predict the observed pressure depletion trends.

2. Methodology

The workflow modified for this study (Fig. 3) includes well log interpretation, rock physics modelling, data analysis, seismic interpretation, AVA, prestack inversion (relative and full spectrum), and seismic attributes.
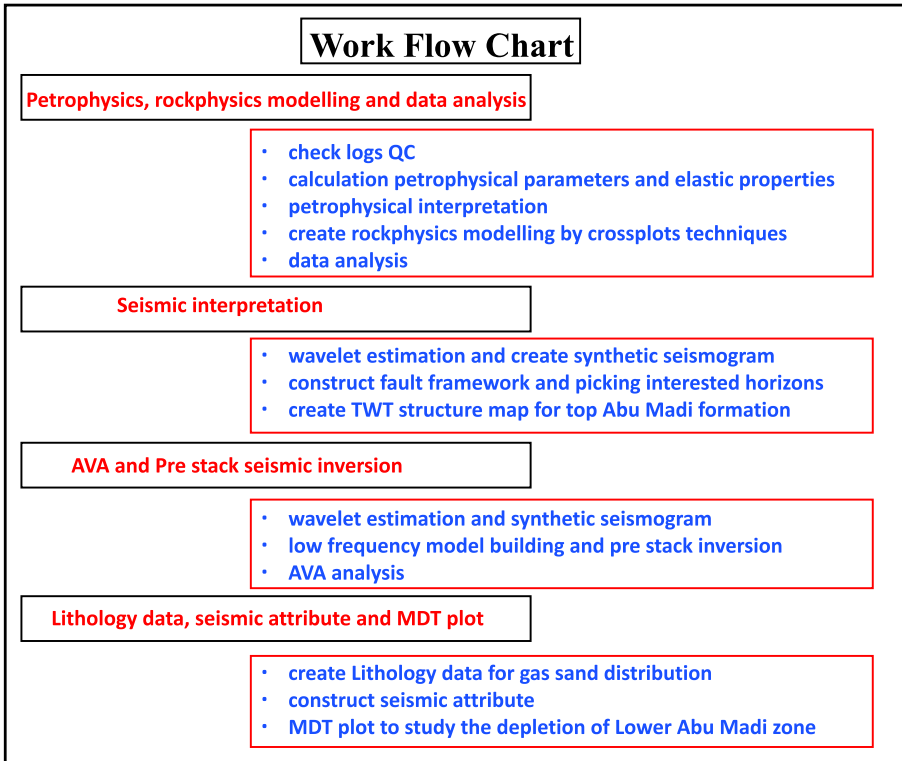

Work Flow Chart

Petrophysics, rockphysics modelling and data analysis

- check logs QC
- calculation petrophysical parameters and elastic properties
- petrophysical interpretation
- create rockphysics modelling by crossplots techniques
- data analysis

Seismic interpretation

- wavelet estimation and create synthetic seismogram
- construct fault framework and picking interested horizons
- create TWT structure map for top Abu Madi formation

AVA and Pre stack seismic inversion

- wavelet estimation and synthetic seismogram
- low frequency model building and pre stack inversion
- AVA analysis

Lithology data, seismic attribute and MDT plot

- create Lithology data for gas sand distribution
- construct seismic attribute
- MDT plot to study the depletion of Lower Abu Madi zone

Fig. 3. Work flow chart.

2.1. Well log interpretation

There are four wells in the study area (Fig. 2) A, B, C, and D that encounter the Abu Madi Formation. Well logging data included original log

data (gamma-ray GR, Density, Neutron, Sonic (compressional and sonic) log, Resistivity) and calculated data (water saturation, effective porosity, and shale volume), which were calculated using Techlog software v2015. The log interpretation helps in understanding the petrophysical parameters of the reservoir. A qualitative and quantitative interpretation was applied for all available well data. Evaluation of petrophysical properties of subsurface formations, which involve shale volume was calculated by neutron and density logs:

$$V_{sh} = \frac{\Phi_N - \Phi_D}{\Phi_{Nsh} - \Phi_{Dsh}},$$

effective porosity was calculated (by using total porosity Φ_{Nd} from density and neutron logs):

$$\Phi_{Nd} = \frac{(\Phi_N + \Phi_d)}{2},$$

and shale volume Φ_{eff} (*Schlumberger, 1972*):

$$\Phi_{eff} = \Phi_{Nd} * (1 - V_{sh}),$$

water saturation is calculated by using Indonesia equation which Abu Madi formation is unclean formation also the acoustic and elastic properties such as (Vp, Vs, P-impedance (P-imp), S-impedance (S-imp), Vp/Vs ratio, poisson's ratio, and shear modulus) were calculated using Techlog software (v2015) (by elastic properties from precomputation module) using shear, compressional, and density logs input data. The Quanti Elan (lithology saturation model) was calculated for each well to determine reservoir characteristics and to show the vertical distribution of the hydrocarbon occurrences within the zones of interest of the Upper Abu Madi and Lower Abu Madi members (UAM & LAM).

Well logging and formation evaluation analysis aim to detect and evaluate new productive horizons for the formation (*Schlumberger, 1974*). Well A is located in the northeastern part of the study area and it lies 780 m north of well B. Well A interpretation is displayed on nine tracks (Fig. 4). The first track represents the measured depth (MD) in meters. The second track represents the zonation. The third track represents the sand intervals or subzones in the Abu Madi reservoir, which is subdivided into sand
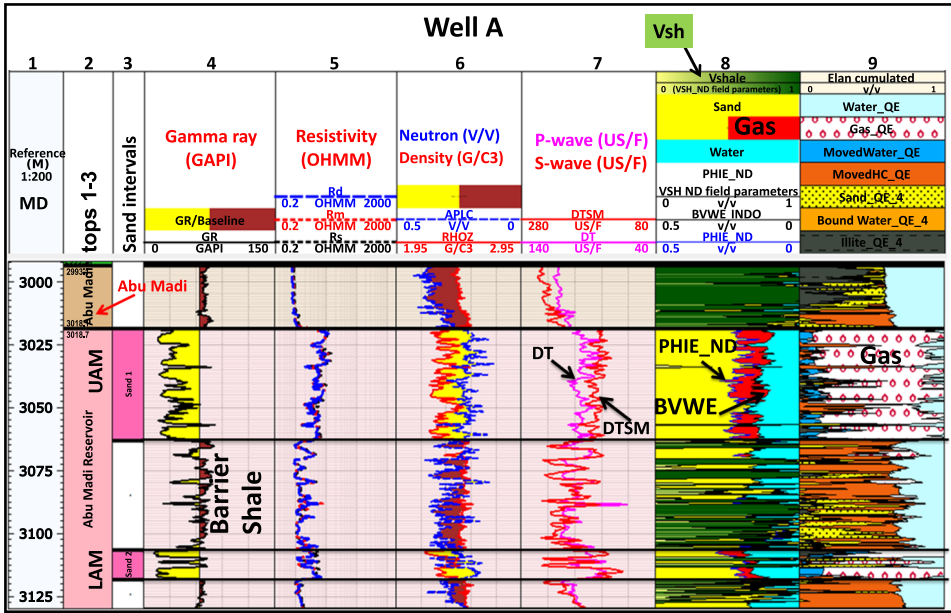
Fig. 4. Petrophysical analysis for well A.

layers (Upper Abu Madi and Lower Abu Madi separated by shale). The fourth track represents the gamma-ray (GR) log and it confirms that there are two sand layers separated by shale. The fifth track represents the resistivity curves of the shallow, medium, and deep resistivity logs (Rs, Rm, and Rd) on a logarithmic grid. The sixth track represents density (RHOZ) and neutron (APLC) and their shading to differentiate between shale and sand intervals and they show a large crossover due to the presence of gas (gas signature) in sand intervals. The seventh track represents shear and compressional logs (DTp and DTs); these logs show crossover sand intervals between them. The eighth track shows the effective porosity (PHIE), bulk water volume (BVWE), and volume of shale. The area between the effective porosity and bulk volume of water is related to the gas amount. The ninth track represents the Quanti Elan or litho saturation model by using effective porosity, the volume of shale, and water saturation as data output (the data output is the ratio of lithology and fluid for each zone) and shows that the lithology of formation is sand and shale with the presence of gas at sand intervals in Abu Madi Reservoir. According to the available data, the Abu

214

Madi Formation was encountered at 3018 m (measured depth MD) with an effective average porosity of 23.4% and average water saturation (Sw) of 40.6%. The reservoir of this interval is mainly characterized by sand with thin streaks of shale and siltstone. The Abu Madi Formation has almost the same characteristics in the four wells.

The geological well log correlation after *Vaughan et al. (2014)* (Fig. 5) shows the stratigraphic relationships between the Upper Abu Madi Reservoir (original pressure) and Lower Abu Madi Reservoir (pressure depleted).
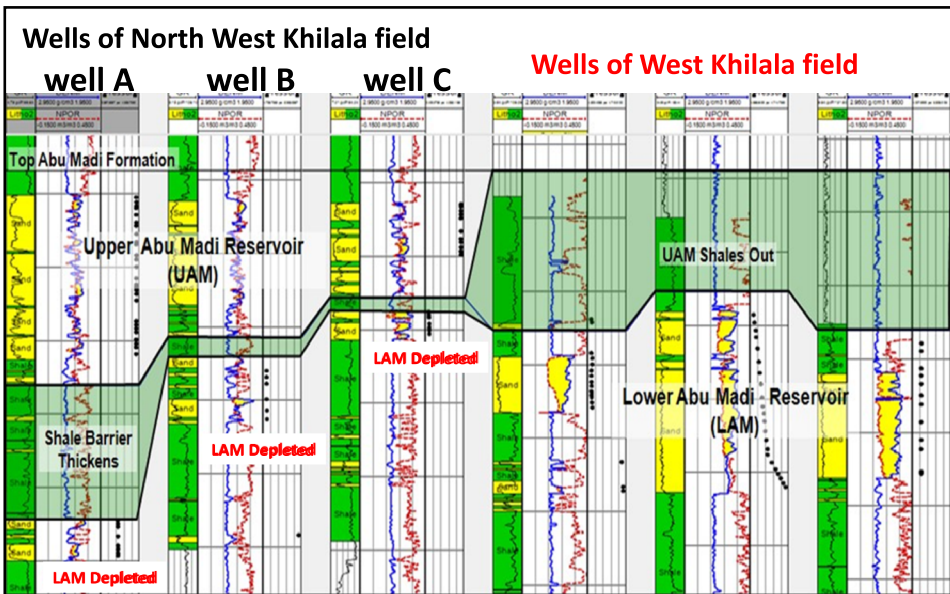
Fig. 5. Geological well log correlation in the field (after *Vaughan et al., 2014*).

2.2. Rock physics modelling

Rock physics models are used as a significant tool in reservoir characterization. Rock physics draws a relationship between geology and seismic data. It helps to explain reflection signatures by quantifying the elastic properties of rocks and fluids. By creating models, it can help us to understand the characteristics of reservoir and non-reservoir zones (*Ødegaard and Avseth, 2004*). Cross-plotting has been used in rock physics analysis because it allows a fast and expressive evaluation of attributes (*Castagna and Swan,*

1997). It can easily discriminate between different lithology units and fluid types within the cross-plot space, which aids in making a direct interpretation. Cross-plotting of different parameters is a great tool for visual analysis is helpful in marking the data clusters in the target zones (*White, 1991*). Based on their response, these data clusters can be classified into different lithologies/facies (*Mavko et al., 2009*). In addition, the resultant model provides clear discrimination between non-reservoir shales and reservoir sands and bridges between elastic properties (P-wave velocity, S-wave velocity, density, impedance, and VP/VS ratio) and reservoir properties (porosity, permeability, and saturation) (*Avseth, 2000; Chi and Han, 2009*). Therefore, the available well logs of the wells in the study area were successfully cross-plotted, in order to determine the characteristics of the reservoir and discriminate between different lithologies and fluids.

Cross-plots of P-impedance (P-imp) vs. S-impedance (S-imp), Lambda Rho vs. Mue Rho ($\lambda\rho$ vs. $\mu\rho$) are calculated using log transform module in Hampson-Russell software (v10) and Vp/Vs ratio vs. P-impedance (P-imp) were successfully generated by using four wells A, B, C, D (Fig. 6), (Fig. 7), and (Fig. 8), respectively.

P-impedance (P-imp = $Vp * \rho$) and S-impedance (S-imp = $Vs * \rho$) (*Gadallah and Fisher, 2009*) cross-plots are common techniques for lithology and
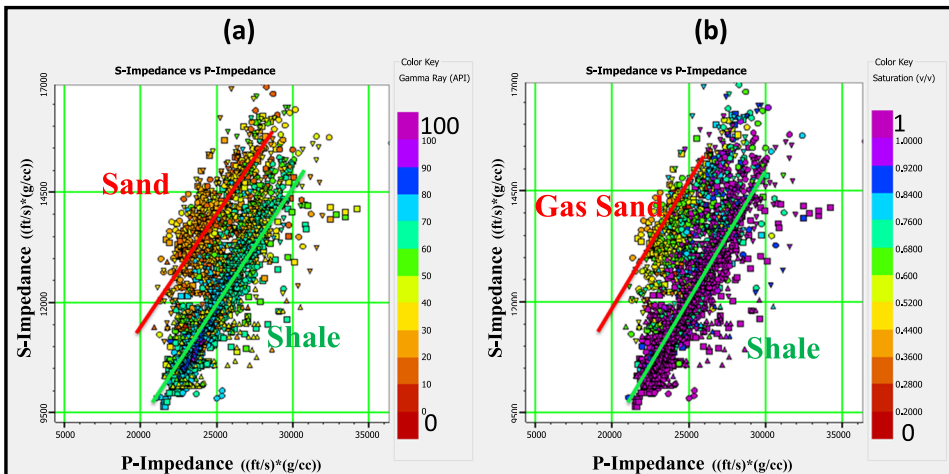

Fig. 6. A cross-plot applied for all wells between P-imp versus S-imp coloured by gamma rays (a) water saturation (b).
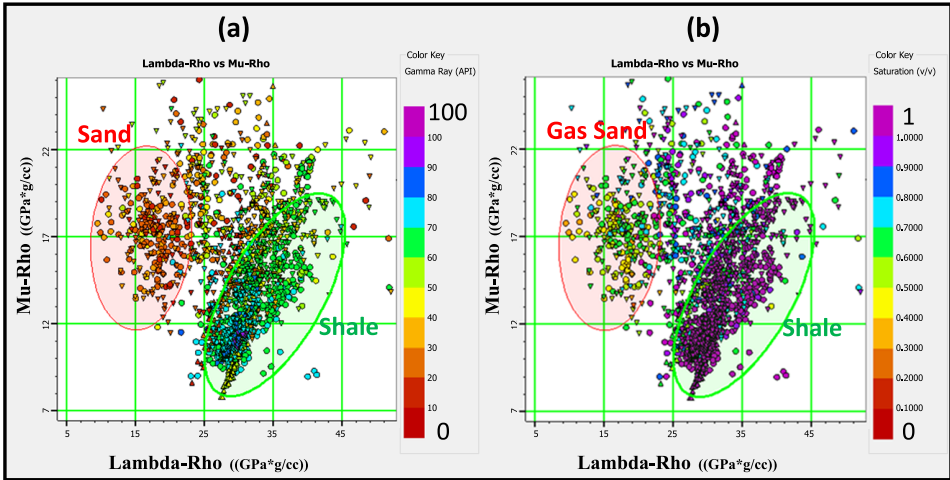
216

Fig. 7. A cross-plot applied for all wells between $\lambda\rho$ versus $\mu\rho$ coloured by gamma rays (a) water saturation (b).
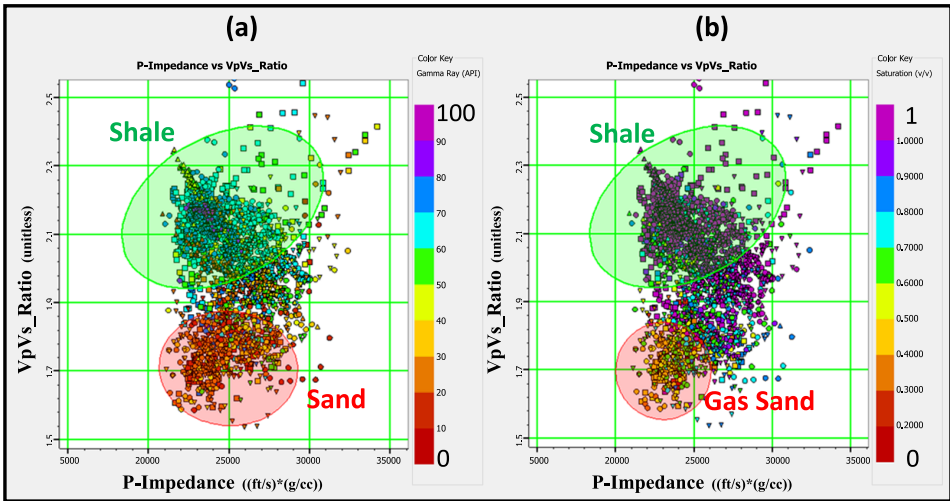

Fig. 8. A cross-plot applied for all wells between P-imp versus VP/VS ratio coloured by gamma rays (a) water saturation (b).

fluid prediction. Figure 6 shows the P-imp – S-imp cross-plot for the four wells, S-imp is plotted on the y-axis and P imp is plotted on the x-axis coloured by gamma rays (Fig. 6a) and water saturation (Fig. 6b). The gas

sand area is represented by the red polygon. Shale is presented by a green polygon.

Rock properties can be extracted from the relationship between Lamé parameters λ, μ (Mu) (rigidity) and ρ (density) and their ability to perform inversion (*Goodway et al., 1997*). The relationship of Mu-Rho or rigidity is related to the rock matrix, so it can be used for lithology discrimination. High rigidity is usually associated with sandstone because the dominant mineral in the sand matrix is quartz, which is characterized by a higher value of Mu-Rho than shale. Fluid content can be distinguished by using incompressibility or Lambda-Rho, where the density of sandstone containing hydrocarbons is less than the density of sandstone containing water. As a result, in sand zones containing hydrocarbons, the Lambda-Rho values are low. It should be considered that neither λ nor μ are powerful and accurate indicators individually; however, the combination of λ and μ exerts a direct indicator for both lithology and fluid content (*Al-Dabagh and Alkhafaf, 2011*).

Figure 7 shows the $\lambda\rho$ vs. $\mu\rho$ cross-plot for the four wells, $\mu\rho$ is plotted on the y-axis and $\lambda\rho$ is plotted on the x-axis coloured by gamma rays (Fig. 7a) and water saturation (Fig. 7b). The sand reservoir zones are marked with a red polygon in the cross-plot, which corresponds to a low $\lambda\rho$ value and a high $\mu\rho$ value well. Gas sand has a low difference value while shale has a higher value. The results confirmed that this method can be used with confidence to characterize reservoirs and to separate gas-bearing sandstone reservoirs from shale.

Figure 8 shows the Vp/Vs – P-imp cross-plot for all wells, Vp/Vs is plotted on the y-axis and P-imp is plotted on the x-axis coloured by gamma rays (Fig. 8a) and water saturation (Fig. 8b). A cross-plot of P-impedance versus Vp/Vs from which sand and shale can be discriminated. This figure shows two clusters in the cross-plot domain and could separate lithology and pore fluid. The gas sand area with low values of Vp/Vs and acoustic impedance is represented by the red polygon. Shale is represented by a green polygon with a high value of Vp/Vs and acoustic impedance.

2.3. Data analysis

Since the cross-plotting of well logs in the study area could successfully discriminate between different lithologies and fluids, therefore data analysis

will indicate wether the seismic resolution could show the differences as well or not. Data analysis is a powerful tool to show that the integration between seismic data and well log data is successful. A filtered log to the seismic frequency is applied on the same logs that were used in the rock physics model to provide that the seismic resolution can discriminate between reservoirs and non-reservoirs, to confirm that the inversion process will consequently be successful (by using Hampson-Russell software v10, (log processing then select log math then frequency-filter module). A frequency filter was ap-
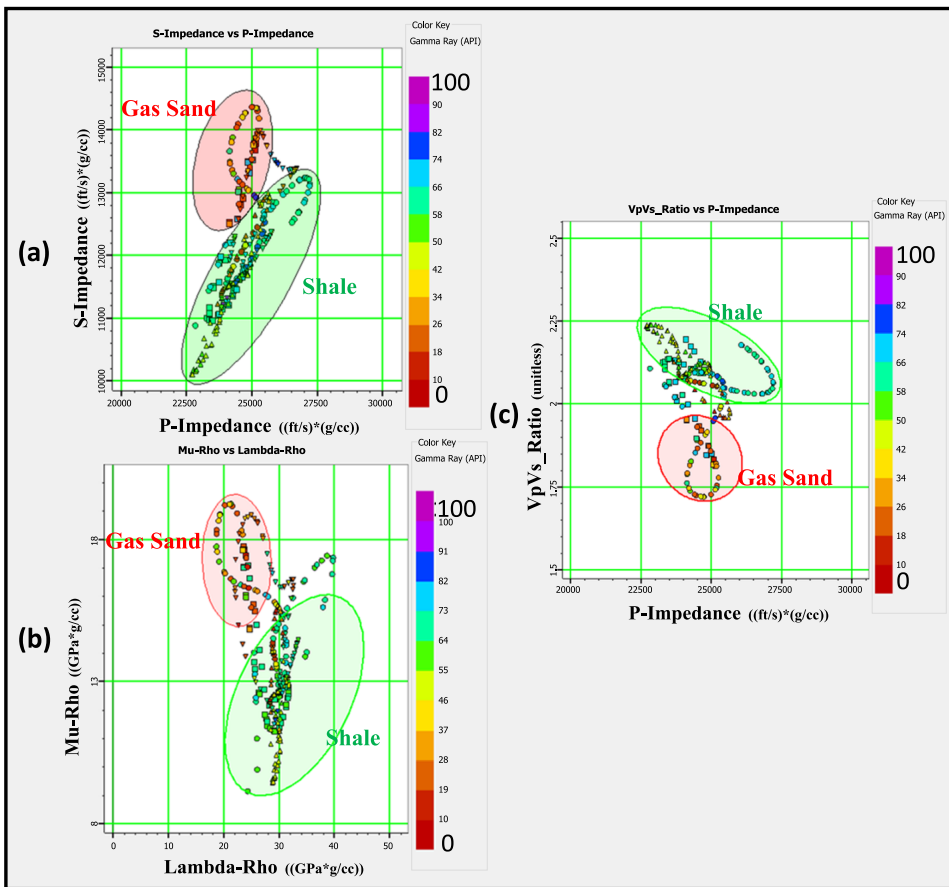

Fig. 9. (a) Filtered P-impedance versus S-impedance cross-plot; (b) Filtered $\lambda\rho$ versus $\mu\rho$ cross-plot; (c) Filtered P-impedance versus VP/VS ratio cross-plot. All cross-plots are coloured by gamma rays.

plied on the same logs by the frequency range of seismic data (8–45 Hz), which were used in the rock physics model and were cross plotted by using the same template (Fig. 9).

2.4. Seismic interpretation

Seismic interpretation included a detailed analysis of the available 2D reflection seismic profiles covering the study area (Fig. 2). The acquisition parameters of the seismic survey and the processing sequence were applied to the seismic data shown in Fig. 10 and Fig. 11, respectively, to assess the hydrocarbon potential and delineate the best locations for drilling wells (*Gadallah and Fisher, 2009*). Seismic data were tied to the wells by using density and calibrated sonic logs, in addition to extracted wavelets. In this

Spread Geometry	
Spread	Symmetrical split-spread, receivers oriented N–S
Shooting Geometry	Orthogonal, 1 line roll, brick pattern
In-line Offsets	4975 m – 25 m – 25 m – 4975 m
Receiver Lines/Swath	10
Channels per line	200
Full Spread	2000 channels
Receiver point Spacing	50 m
Receiver line Spacing	350 m
Source point spacing	50 m
Source line spacing	350 m, 175 m inline stagger between adjacent swathes
Number of VP's/Salvo	7
Nominal Fold	70/72 (striped)
Inline Roll	350 m
Cross-line Roll	350 (1 receiver line)
Source type	Dynamite
Recording length	8 s
Sample rate	2 ms

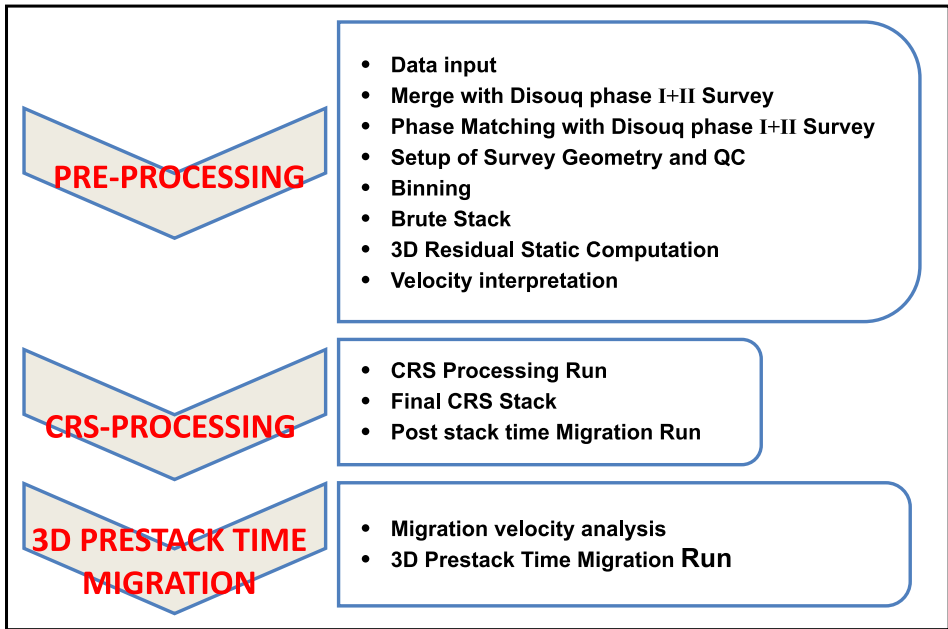Fig. 10. A list of all recording, spread, sensor, and source parameters.
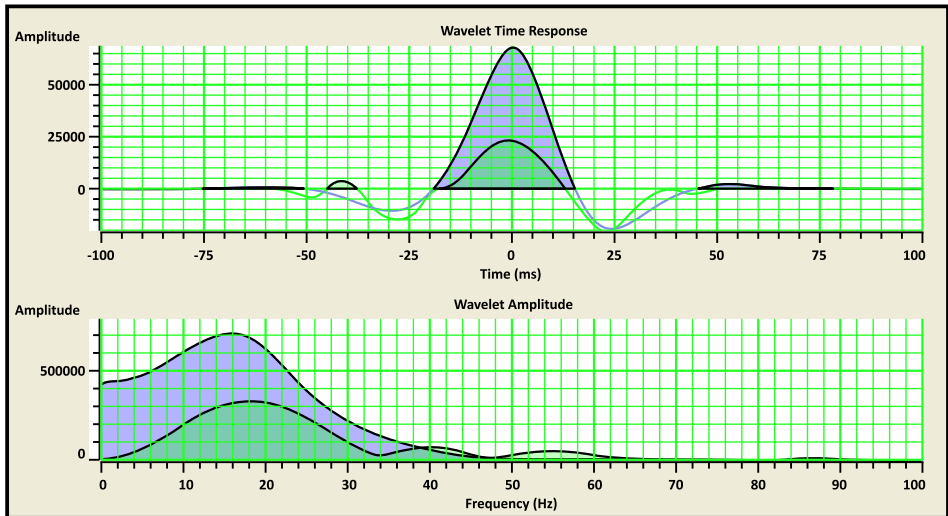
Fig. 11. The applied processing sequence.

Fig. 12. The extracted wavelet group.

study, a deterministic wavelet was extracted by using well C from near- and far-data offset seismic data. A wavelet group was created by combining extracted wavelets from near and far offset data (Fig. 12). In this study, seismic data are normal polarity and zero phases. A synthetic seismogram

Fig. 13. Synthetic seismogram.

Fig. 14. Interpreted E–W seismic section IL 51380.

was generated and matched the gathered group seismic data (Fig. 13). The horizons of interest which were picked:

(1) AM: Top Abu Madi Formation;

(2) Shale: A body of shale between two sand bodies (upper and lower Abu Madi sands) within Abu Madi;

(3) Base: the base of lower Abu Madi sand.

They were corresponding to peak.

    The study area is characterized by a 3-way dip closure structure against a N–S- to NNW–SSE trending fault (F1: en echelon normal faults downthrown to the east and northeast). The top and lateral seals of the Abu Madi closure are provided by shales of the lower Pliocene. All wells in the study area were drilled according to structural traps. There are F2 and F3 which have the same trend as F1 NNW–SSE. The study area is affected by several major faults, such as F1, F2, and F3 (Fig. 14). A TWT structure map of the top Abu Madi formation was generated (Fig. 15).
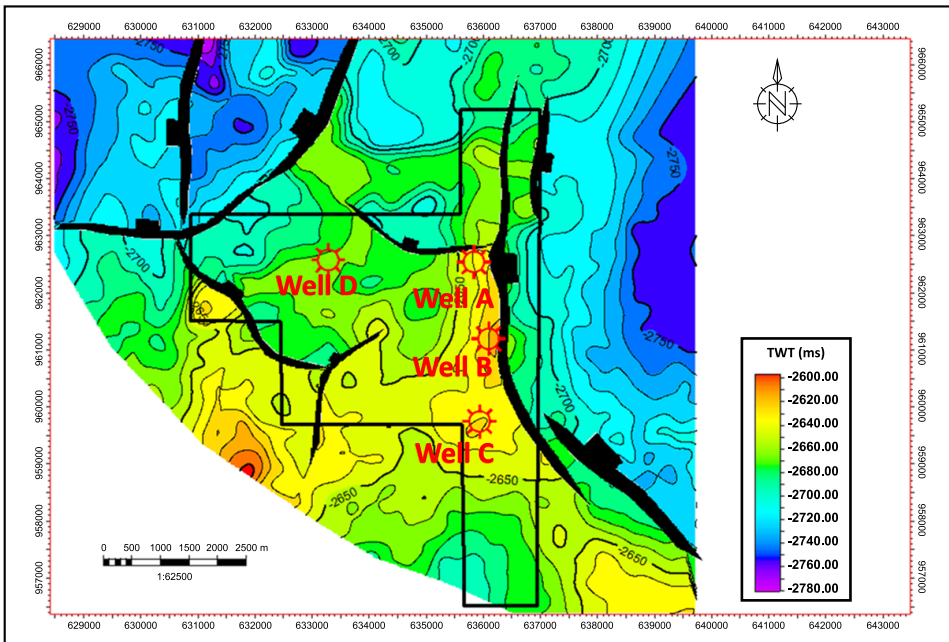

Fig. 15. Two way time structure map for top Abu Madi formation.

2.5. AVA and Prestack Inversion (relative and full spectrum)

Amplitude versus angle (AVA) and seismic inversion are the most widely used and successful tools applied for lithology and fluid discrimination. AVA is used in direct hydrocarbon exploration using prestack seismic data amplitudes to improve reservoir forecasting in the petroleum industry. Practical AVA analysis of seismic reflection data was introduced in the literature in the early 1980s (*Backus et al., 1982; Ostrander, 1982, 1984*).

The AVA response is classified into four classes after *Rutherford and Williams (1989)* and *Castagna et al. (1998)*. Class I is a high-impedance gas sandstone reservoir covered by shale, and class II and IIp (reversal Polarity) are gas sandstone reservoirs with a small acoustic impedance contrast of nearly zero contrast in impedance (a low intercept value and a strongly negative gradient). Class III gas sand reservoirs have lower impedance than the covering medium, and the classic bright spot sand that is described by stronger reflection relative to the surrounding reflectors. Class IV (weak bright spots) is a low impedance gas sandstone reservoir, but large negative amplitude is shown by such sands at zero offset and then decrease slightly with increasing offset is sand). The AVA response of a reflector is described by two parameters: intercept or reflectivity (amplitude) at zero offset and the gradient of the amplitude variation with offset. These two parameters are often referred to as A and B or Ro and G. This broadband method includes phase and spectral changes over the partial stacks using Aki-Richards and Zoeppritz AVA modelling. AVA reflection coefficient curves (amplitude-offset or angle) were classified by *Rutherford and Williams (1989)* for gas sand into four classes. This classification was developed in gas-saturated reservoirs.

In the study area AVA analysis is performed at the top of the Abu Madi reservoir, the forward modelling of AVA responses is normally the greatest way to start an AVA analysis. Therefore, the shear and compressional sonic logs in addition to the density log are used to estimate the impedance and reflectivity series. The reflectivity series is convolved with the extracted wavelet to generate a synthetic seismogram. The synthetic seismogram is correlated with the real seismic data. The next step was to perform the AVA analysis, which had as the main target, to characterize the reservoir seismic response and its relationship with the seismic amplitude. Cross-plotting the intercept vs. gradient in real gathers helped in achieving the goal. It

is very important to identify the range of incident angles, in addition to selecting the horizons of interest. This analysis was performed at incident angles of 45 degrees and the approximation of Aki-Richards. AVA Workflow is (using Hampson-Russell (v10) software) 1-Wavelets Extraction (Fig. 12) 2-Synthetic Generation (Fig. 13) 3-AVO analysis (Fig. 16).
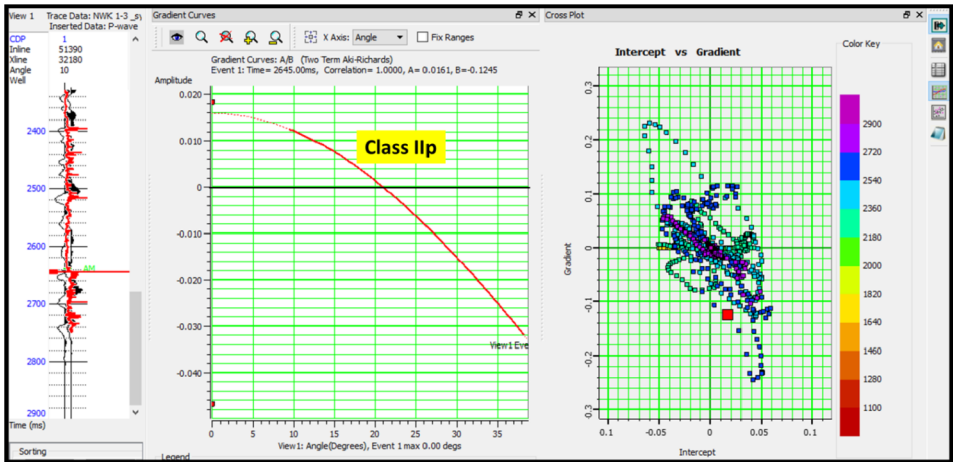

Fig. 16. AVA Analysis for well A shows that AVA response for top Abu Madi reservoir is class 2p.

The top of the Abu Madi reflector was picked at each well, and their amplitudes were plotted against the angles to monitor their AVA response and to determine which class of AVA they belong to, this was successfully accomplished by using Hamson Russel (v10) software deployed to analyse the present AVA data. The top of the Abu Madi reservoir was selected considering a negative reflector (trough).

It has a positive intercept and a negative gradient. The polarity changes with offset (Fig. 16), owing to the phase reversal that is inherent in this response, the AVA effect leads to high negative amplitudes at far offsets. Generally, it is found in moderately compacted and consolidated sediments when the acoustic impedance of the gas sand and the encasing shale are nearly equal *Ross and Kinman (1995)*. A common tool to interpret prospective AVA anomalies and how they relate to background trends is cross-plotting of AVA attributes (i.e., the intercept versus gradient cross-plot). This helps in determining the potential hydrocarbon AVA responses and how they relate

to the appropriate geologic setting (*Castagna and Swan, 1997; Castagna et al., 1998; Ross, 2000*).

Seismic inversion is the process that can be used to estimate the acoustic impedance and elastic parameters from broad-band seismic reflections (reflectivities). Acoustic impedance is an essential physical property of rocks and helps us in subsurface studies, which allows suitable interpretation of seismic data in geologic terms, because variations in acoustic impedance should relate to vertical and lateral variations in lithology. The conversion of seismic traces into acoustic-impedance logs was first reported by *Lavergne (1975)*, *Lindseth (1976)*, *Lavergne and Willm (1977)*, and *Lindseth (1979)*.

Prestack seismic inversion is the type of inversion that is applied to the prestack datasets, either CMP gathers or angle stacks. The advantage of
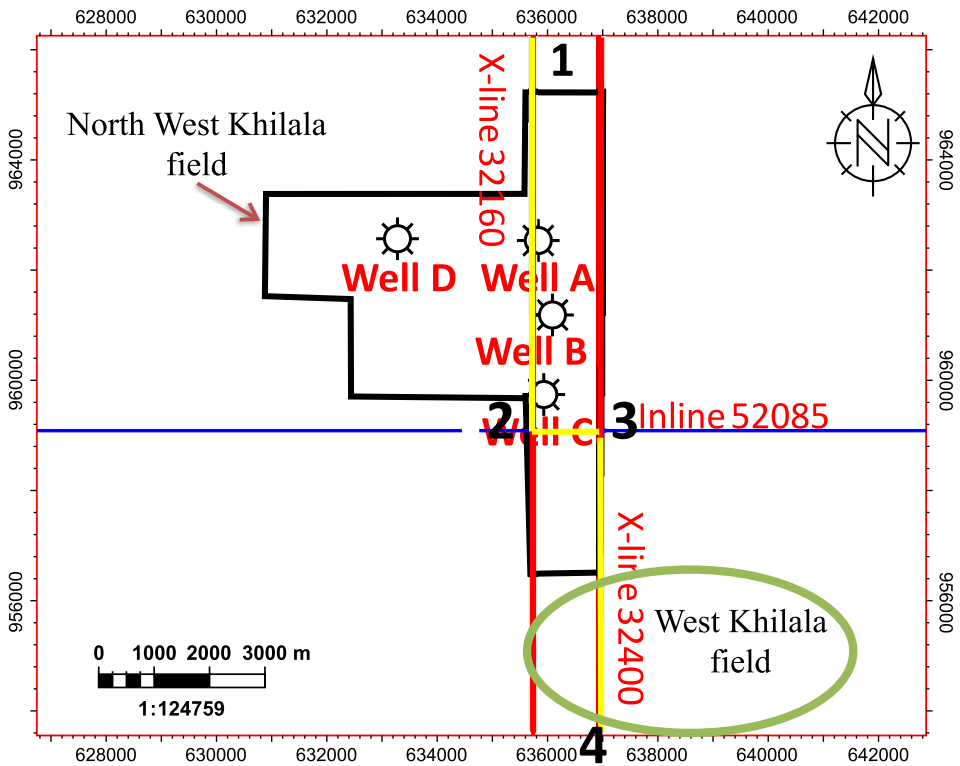

Fig. 17. The selected seismic line.

working with prestack data is the fact that the low-frequency components of interval velocity are implicit in the move-out curves. In addition, nonzero incidence seismic waves can also be converted to S-wave impedance, giving us the opportunity to estimate elastic parameters using the full elastic earth model. These elastic parameters, within good petrophysical and well control, provide lithology and aid properties from the reservoir (*Chopra and Marfurt, 2007*).

Relative and full-spectrum prestack inversion was applied in the case study. This process required one or more well logs, a 2D prestack seismic data, which is usually in the form of fully processed CDP gathers or angle gathers, and a set of horizons to guide the interpolation of the initial guess model (Hamsson Russel (v10) manual). In this study, we used 2D angle gather group prestack seismic data.

The typical workflow for prestack inversion consists of the following steps:

(1) Load wells.
(2) Load seismic data.
(3) Load horizons or pick horizons.
(4) Correlate each well with the seismic volume to optimize the depth-to-time conversion. At the same time, extract one or more wavelets.
(5) Build an initial model for inversion.
(6) Run inversion analysis to determine inversion parameters.
(7) Run inversion over the data, and analyse the results.

The output data, for the prestack inversion are four outputs: acoustic impedance, shear impedance, Vp/Vs ratio and density. The process aims to monitor the lateral variations in the physical properties of the reservoir.

Well log data provide low-frequency inferred information under the bandwidth of the seismic data. This project inverted 2 angle stacks (5–15 and 37–42 degrees) to gather group data to produce P-impedance, Vp/Vs, and density (relative and absolute products). The Abu Madi reservoirs have a poor P-impedance contrast with the shales above and below, making this parameter insensitive to reservoir prediction. However, Vp/Vs data could differentiate between the non-reservoir shale and reservoir sand. The use of the ratio of compressional wave velocity to shear wave velocity, Vp/Vs, is a good tool in identifying fluid type. The fact that compressional wave velocity decreases and shear wave velocity increases with the increase of gas hydrocarbon saturation, makes the ratio of Vp/Vs more sensitive to
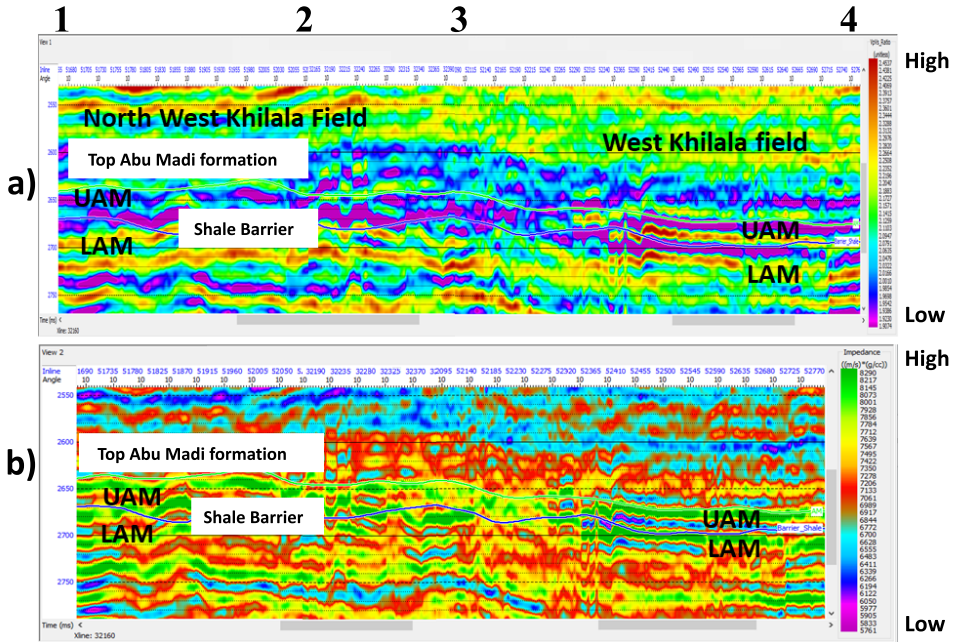
Fig. 18. The intersection line for (a) full spectrum (absolute) Vp/Vs ratio inverted, (b) absolute acoustic impedance.

change of fluid type than the use of Vp or Vs separately (*Hamada, 2004*). AN intersection seismic line (Fig. 17) was selected to monitor the lateral variations in the Lower Abu Madi Formation by using the output results of the relative and full spectrum (Figs. 18 and 19) Vp/Vs ratio and acoustic impedance Zp.

The separation of sands and shales in the Vp/Vs domain allowed for accurate mapping of the intraformational shale between the Upper Abu Madi and Lower Abu Madi reservoirs and refinement of the top Abu Madi Formation flooding surface interpretation (*Vaughan et al., 2014*).

2.6. Seismic attributes

Seismic attributes are very important information that can be extracted from seismic data. To investigate the probability and delineate the distribution of gas sand within UAM and LAM, a maximum magnitude surface attribute was applied to the lithology data.
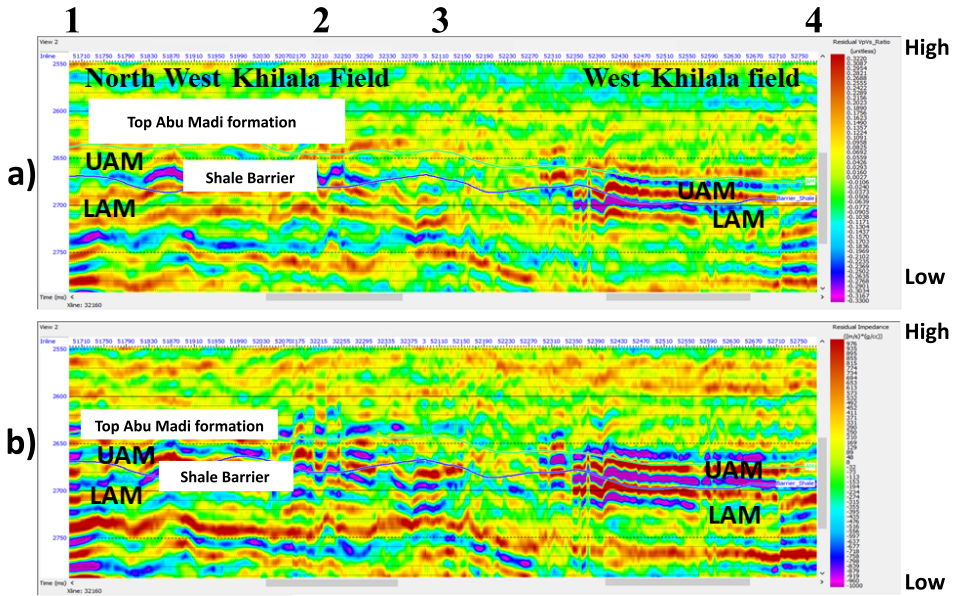
Fig. 19. The intersection line for (a) the inverted relative Vp/Vs ratio, (b) the relative acoustic impedance.

2.7. Workflow to create lithology data from inverted seismic data

As mentioned in the rock physics section, the cross-plot of the P-imp and Vp/Vs ratios from well log data could successfully discriminate between different lithologies and showed two clusters of gas sand and shale. The zone set of gas sand cluster was copied and projected on the P-imp and Vp/Vs ratio cross-plot, which was generated from the seismic inverted data. Therefore, Lithology data (Fig. 20) was created. This was successfully done by using the copy module in HR software.

Max magnitude surface attribute had been applied on lithology data between two layers (Abu Madi and shale) by using Petrel software 2017 for upper Abu Madi an also Max magnitude surface attribute had been applied on lithology data between two layers (shale and base for lower Abu Madi) for lower Abu Madi. Max magnitude surface attributes were extracted from the resulting lithology data for both the upper and lower Abu Madi formations (Figs. 21 and 22, respectively) to investigate the distribution and areal extension of gas sand within the study area by using Petrel software 2017.
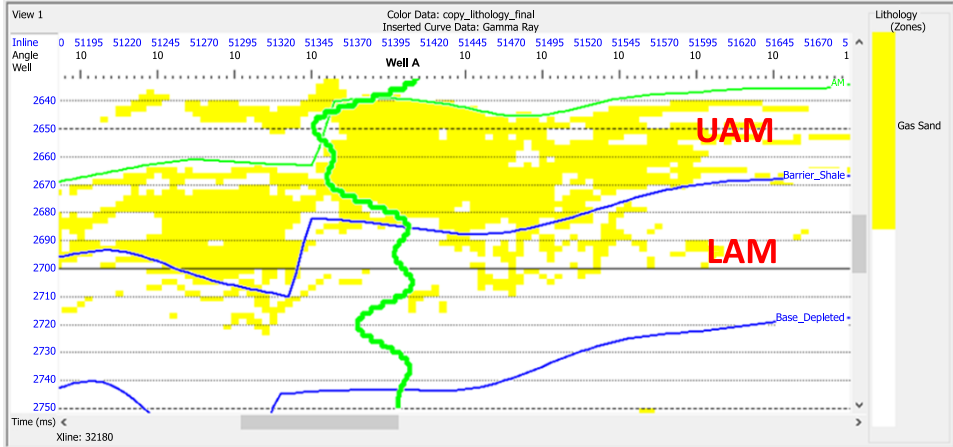
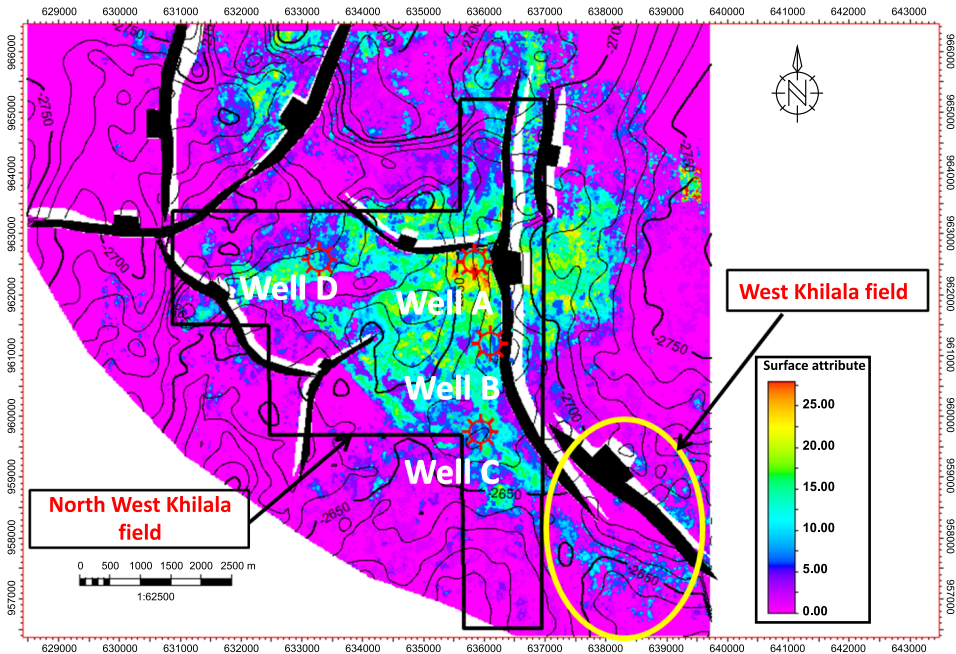Fig. 20. Cross section at well A, lithology gas sand distribution.

Fig. 21. Max magnitude surface attribute was applied to lithology data for the upper Abu Madi to show the distribution of gas sand.
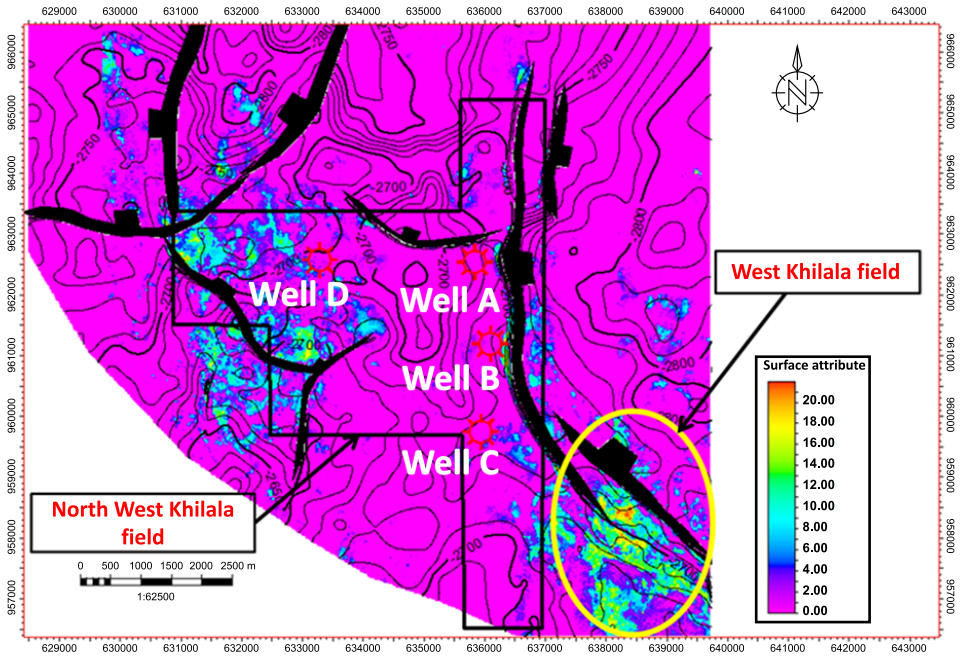
Fig. 22. Max magnitude surface attribute was applied to lithology data for lower Abu Madi to show the distribution of gas sand.

2.8. Modular dynamic formation tester (MDT) pressure data

The modular dynamic formation tester (MDT) is the tool that can be used to test the formation and measure the formation pressure and temperature. MDT data were used to investigate the pressure communication of the Abu Madi Formation. The MDT pressure plot (Fig. 23), showed that the pressure at UAM ranges 4700–4800 psi at the three wells, while the pressure of the LAM varies at different well locations.

3. Results

The well data are interpreted to investigate the petrophysical parameters of the Abu Madi reservoir, which is subdivided into upper and lower Abu Madi sand intervals separated by shale layers (Abu Madi Formation is characterized by an average effective porosity of 23%, average saturation
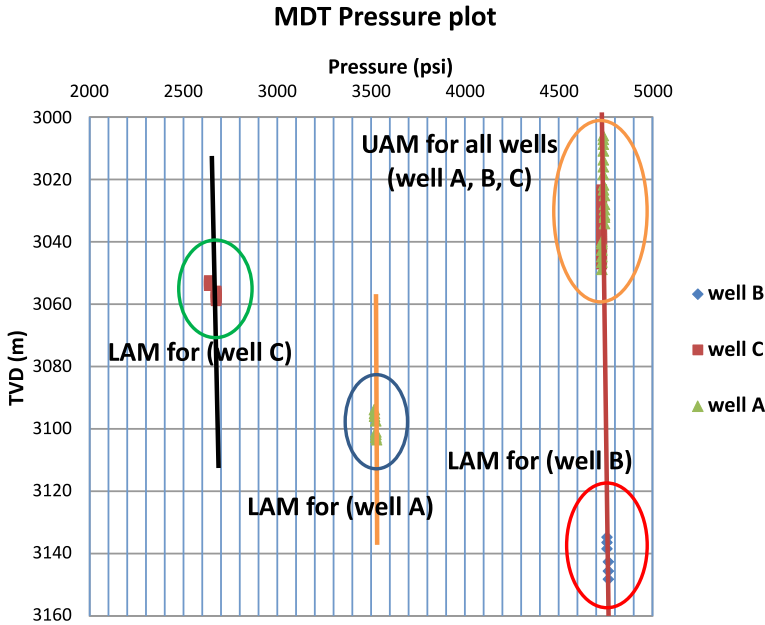
Fig. 23. MDT pressure plot for well A, B, C.

of 40%, average volume of shale of 10% and net pay of 10 m).

Well log correlation (Fig. 5, after *Vaughan et al., 2014*) shows that the UAM reservoir shales out laterally, while the LAM reservoir thins laterally. Wells shows subtle variations in the UAM Reservoir. Cross-plotting is a widely used technique in rock physics analysis. Fig. 6 shows the P-imp – S-imp cross-plot for the four wells, S imp is plotted on the *y*-axis and P-imp is plotted on the *x*-axis. It shows two clusters in the cross-plot domain and could separate lithology and pore fluid. The gas sand areas with low values of S-imp and P-imp are represented by red polygons and the presence of gas decreases the S-impedance. Shale is presented by a green polygon with a high value of P and S-impedances.

In the $\lambda\rho$ vs. $\mu\rho$ cross-plot (Fig. 7), the gas sand reservoir zones are captured with a red polygon in the cross-plot, which corresponds to a low $\lambda\rho$ value and a high $\mu\rho$ value. The results confirmed that this method can be used with confidence to characterize a reservoir and to separate gas-bearing

sandstone reservoirs from shale. Gas sand has a low ratio and low difference value while shale has a higher value.

A cross-plot of P-impedance versus Vp/Vs (Fig. 8) was generated to discriminate between different lithologies and different fluids (the separation between gas sand and shale). It shows two clusters in the cross-plot domain and separate lithologies and pore fluids. The gas sand area with low values of Vp/Vs and P-impedance is represented by the red polygon. Shale is presented by a green polygon with a high value of Vp/Vs and acoustic impedance.

In the study area, the AVA suggested small positive responses classified as class IIp (Fig. 16), owing to the phase reversal in which the AVA effect leads to high negative amplitudes at far offsets. They were projected in the class IIp zone with intercept value = 0.02 and gradient value = −0.12. The NWKh field closure comprises a 3 way dip structure against a N–S to NNW–SSE trending echelon normal fault downthrown to the east and northeast.

Max magnitude seismic attributes maps (Figs. 21 and 22) clearly show sediment dispersal patterns originating from the south and fanningout to the north and northeast around the subject field. The UAM is characterized by high amplitude in the NWKh field, while the LAM is characterized by lower amplitude in the NWKh field and high amplitude in the WKh field. AVA and seismic attribute extractions of the reservoir interval itself, display lobe-shaped morphologies suggesting that the stacked sands laterally pinch out to the north, south, and east. Individual sand body correlations are difficult to determine, but intraformational shale is more easily correlated across the field. MDT pressure data for wells A, B and C in the northwestern Khilala field (Fig. 23) show that the three wells are in pressure communication at UAM, while at LAM, the three wells have different pressure trends. The MDT pressure plot shows the vertical depletion for Lower Abu Madi, and the maximum magnitude seismic attribute show the lateral depletion.

4. Discussion

One significant shale layer subdivides the Abu Madi reservoirs into upper and lower levels. The Abu Madi reservoirs have a poor P-impedance dif-

ference from the shales above and below, making this parameter insensitive to reservoir determination, as it is classified as class IIp. However, Vp/Vs data more clearly differentiate between the non-reservoir shale and reservoir sands. The max magnitude seismic attribute extracted maps showed the variation of amplitude values between UAM and LAM in both NWKh and WKh fields, and the distribution and presence of gas, in addition to the depletion of lower Abu Madi sand in North West Khilala (NWKh) field and presence of gas in West Khilala (WKh) field.

The pressure depletion was investigated laterally and vertically by a relative/full spectrum inversion and MDT pressure data, respectively. The MDT data helped to understand the variation in the amplitudes and depletion of LAM formation in the North West Khilala field. Two wells showed the depletion in the lower Abu Madi. This depletion was due to communication with the West Khilala field, which was produced from the lower Abu Madi Reservoir in 2007.

5. Conclusion

This study is focused on the North West Khilala field. It is a gas field located on the northern onshore part of the Nile Delta. The main objective of this study is to determine the characteristics of the late Messinian Abu Madi reservoir in the NWKh field and study the depletion of the Lower Abu Madi sand interval. The Abu Madi Formation can be subdivided into upper and lower Abu Madi sand members, which are separated by an intraformational shale layer.

In this study, AVA, seismic inversion (relative and full spectrum), attributes and rock physics models were successfully applied to delineate the reservoir characterization of the Late Messinian Abu Madi Formation in North Western Khilala field. Several gas discoveries were made using these techniques as a direct hydrocarbon indicator (DHI) and risk modification tool. The integration of these techniques helped delineate the overall lateral extent of the field, in addition to generating high-resolution multiple rock property models with the aim of capturing reservoir characterization and the observed pressure trends to study and confirm the depletion of the lower Abu Madi sand interval.

Well logging analysis and formation evaluation of the Abu Madi Formation were examined to determine its petrophysical properties, including effective porosity, shale content, water and hydrocarbon saturation, elastic properties, and the Quanti Elan (lithology saturation model) calculated for each well to determine reservoir characteristics and to show the vertical distribution of hydrocarbon occurrences within the intervals of interest Upper Abu Madi and Lower Abu Madi (UAM & LAM).

The North West Khilala field closure comprises a 3-way dip structure against a N–S- to NNW–SSE-trending echelon normal fault that is downthrown to the east and northeast. AVA analysis performed on the top of the Abu Madi reservoir, suggested a class 2p. Seismic inversion (relative and full spectrum) Vp/Vs data could clearly differentiate between the non-reservoir shale and reservoir sands. The maximum magnitude seismic attribute extracted maps generated from gas sand lithology data showed the variation of amplitude values between UAM and LAM in both NWKh and WKh fields and show the distribution and presence of gas. Understanding the distribution of this pressure is an important goal of this study to explain the observed pressure trends and allow for effective field management. The pressure depletion was investigated laterally and vertically by relative/full spectrum inversion and MDT pressure data, respectively. This depletion was due to communication with the West Khilala field, which was produced from the lower Abu Madi Reservoir in 2007.

References

Abdel Aal A., Price R. J., Vaitl J. D., Sharallow J. A., 1994: Tectonic evolution of the Nile delta, its impact on sedimentation and hydrocarbon potential. In: Proceedings of 12th EGPC Exploration and Production Conference, Cairo, Egypt, **1**, 19–34.

Al-Dabagh H. H., Alkhafaf S., 2011: Comparison of Kρ and $\lambda\rho$ in clastic rocks, A test on two wells with different reservoir-quality stacked sands from West Africa. Lead. Edge, **30**, 9, 986–994, doi: 10.1190/1.3640520.

Avseth P. Å., 2000: Combining rock physics and sedimentology for seismic reservoir characterization of North Sea turbidite systems. PhD. Thesis, Stanford University, CA.

Backus M. M., Nepomuceno F., Cao J.-Z., 1982: The reflection seismogram in a solid layered earth. 52nd Annual International Meeting, SEG, Expanded Abstracts, 218–220, doi: 10.1190/1.1826899.

Castagna J. P., Swan H. W., 1997: Principles of AVO crossplotting. Lead. Edge, **16**, 4, 337–342, doi: 10.1190/1.1437626.

Castagna J. P., Swan H. W., Foster D. J., 1998: Framework for AVO Gradient and Intercept Interpretation. Geophysics, **63**, 3, 948–956, doi: 10.1190/1.1444406.

Chi X.-G., Han D.-H., 2009: Lithology and fluid differentiation using rock physics templates. Lead. Edge, **28**, 1, 60–65, doi: 10.1190/1.3064147.

Chopra S., Marfurt K. J., 2007: Seismic Atrributes for Prospect Identification and Reservoir Charcterization. Society of Exploration Geophysicist (SEG), 481 p., doi: 10.1190/1.9781560801900.

Dolson J. C., Boucher P. J., Siok J., Heppard P. D., 2005: Key challenges to realizing full potential in an emerging giant gas province: Nile Delta/Mediterranean offshore, deep water, Egypt. In: Doré A. G., Vining B. A. (Eds.): Petroleum Geology: North-West Europe and Global Perspectives – Proceedings of the 6th Petroleum Geology Conference, **6**, 607–624, doi: 10.1144/0060607.

EGPC, 1994: Nile Delta, North Sinai fields, discoveries and hydrocarbon potentials (A comprehensive overview). The Egyptian General Petroleum Corporation, Cairo, p. 387.

Gadallah M. R., Fisher R., 2009: Exploration Geophysics. Springer, Berlin, 266 p., doi: 10.1007/978-3-540-85160-8.

Goodway B., Chen T., Downton J., 1997: Improved AVO fluid detection and lithology discrimination using Lame petrophysical parameters; "$\lambda\rho$", "$\mu\rho$", & "λ/μ fluid stack", from P and S inversions. SEG Technical Program Expanded Abstracts, 183–186, doi: 10.1190/1.1885795.

Hamada G. M., 2004: Reservoir Fluids Identification Using Vp/Vs Ratio? Oil Gas Sci. Technol. – Rev. IFP, **59**, 6, 649–654, doi: 10.2516/ogst:2004046.

Lavergne M., 1975: Pseudo-velocity-logs in deep offshore exploration (Pseudo-diagraphies de Vitesse en offshore profound). Geophys. Prospect., **23**, 4, 695–711, doi: 10.1111/j.1365-2478.1975.tb01554.x (in French with English abstract).

Lavergne M., Willm C., 1977: Inversion of seismograms and pseudo velocity logs. Geophys. Prospect., **25**, 2, 231–250, doi: 10.1111/j.1365-2478.1977.tb01165.x.

Lindseth R. O., 1976: Seislog process uses seismic reflection traces. Oil Gas J., **74**, 43, 67–71.

Lindseth R. O., 1979: Synthetic sonic logs—a process for stratigraphic interpretation. Geophysics, **44**, 1, 3–26, doi: 10.1190/1.1440922.

Leila M. L., Moscariello A., Šegvić B., 2019: Depositional facies controls on the diagenesis and reservoir quality of the Messinian Qawasim and Abu Madi formations, onshore Nile Delta, Egypt. Geol. J., **54**, 3, 1797–1813, `doi: 10.1002/gj.3269`.

Mavko G., Mukerji T., Dvorkin J., 2009: The Rock Physics Handbook: Tools for Seismic Analysis of Porous Media 2nd edn., Cambridge University Press, New York, 524 p.

Ødegaard E., Avseth P., 2004: Well log and seismic data analysis using rock physics templates. First Break, **22**, 10, 37–43, `doi: 10.3997/1365-2397.2004017`.

Ostrander W. J., 1982: Plane-wave reflection coefficients for gas sands at non-normal angles of incidence. 52nd Annual International Meeting, SEG Expanded Abstracts, **1**, 216–218.

Ostrander W. J., 1984: Plane-wave reflection coefficients for gas sands at non normal angles of incidence. Geophysics, **49**, 10, 1637–1648, `doi: 10.1190/1.1441571`.

Rizk R., El Alfi M., Zaki A., Castellano P., Serafini G., 2002: Seismic Stratigraphy and Facies Architecture of The Late Messinian Abu Madi Fm. in Baltim Area, N. Nile Delta, Egypt. Abstracts of AAPG International Convention, Cairo, Egypt; October 27–30, 2002.

Ross C. P., 2000: Effective AVO crossplot modeling: A tutorial. Geophysics, **65**, 3, 700–711, `doi: 10.1190/1.1444769`.

Ross C. P., Kinman D. L., 1995: Nonbright-spot AVO: Two examples. Geophysics, **60**, 5, 1398–1408, `doi: 10.1190/1.1443875`.

Rutherford S. R., Williams R. H., 1989: Amplitude versus offset variations in gas sands. Geophysics, **54**, 6, 680–688, `doi: 10.1190/1.1442696`.

Salem A. M., Ketzer J. M., Morad S., Rizk R. R., Al-Aasm I. S., 2005: Diagenesis and reservoir-quality evolution of incised-valley sandstones: Evidence from the Abu Madi gas reservoirs (Upper Miocene), the Nile Delta Basin, Egypt. J. Sediment. Res., **75**, 4, 572–584, `doi: 10.2110/jsr.2005.047`.

Schlumberger, 1972: The Essentials of Log interpretation Practice. France, 14, 154–157 (Services Techniques Schlumberger).

Schlumberger, 1974: Log interpretation, Vol. II, Applications. Paris, France.

Vaughan R. D., Ali M., Mustafa A., Adly T., Sulistiono D., Petrov A., 2014: Vertical and horizontal pressure depletion trends captured by AVA geostatistical inversion conditioned reservoir modeling: An example from Late Messinian lacustrine turbidities reservoirs, Nile Delta, Egypt. International petroleum Technology Conference, Doha, Qatar, January 2014, `doi: 10.2523/IPTC-17514-MS`.

White R. E., 1991: Properties of instantaneous seismic attributes. Lead. Edge, **10**, 7, 26–32, `doi: 10.1190/1.1436827`.